Supporting Information

Ultraporous palladium on flexible graphene-coated carbon fiber paper as high-performance electro-catalysts for the electro-oxidation of ethanol

Montree Sawangphruk*[a,b], Atiweena Krittayavathananon[a] and Natee Chinwipas[a]

1. Chemicals and materials

All chemicals in this study were of analytical grade and used without further purification. They were ethanol (Merck, ≥99.9%), graphite powder (20-40 μm, Sigma Aldrich), D(-)-fructose (99%, Sigma Aldrich), hydrogen peroxide (30%, Merck), palladium (II) nitrate dihydrate (40% Pd basis, Sigma Aldrich), potassium permanganate (99%, Ajax Finechem), sodium hydroxide (Carlo Erba, 97%), sodium nitrate (99.5%, QRec), sulfuric acid (98%, QRec), and activated carbon-supported Pd at 10 wt% loading (Pd-C, Sigma Aldrich). Graphitized CFP with the trade name of SIGRACET® GDL 10 BA (thickness = 400 μm, electrical resistance < 12 mΩ cm^2, and areal weight = 85 g m^{-2}) was obtained from SGL CARBON SE (Germany). Water was purified by using the Milli-Q system (>18 MΩ cm, Millipore).

2. Structural and morphological characterizations

Raman Spectroscopy and Fourier Transform Infrared Spectroscopy (FTIR) were used to characterize the structure of rGO. Raman spectra were recorded on a Senterra Dispersive Raman spectroscope (Bruker Optics, Germany) with a laser excitation wavelength of 514 nm. The rGO powders were placed on a clean SiO_2/Si substrate and were then used for Raman measurement. The FTIR spectra were acquired on a FTIR spectrometer (Perkin Elmer System 2000). The specimens for FTIR measurement were prepared by grinding the dried rGO powder mixed with potassium bromide (KBr) to a fine powder and then compressing under high pressure into thin pellets. Scanning Electron Microscopy (SEM) and Transmission Electron Microscopy (TEM) were employed to characterize the morphology of rGO. The TEM images of samples were made using a JEM 1220 (JEOL Ltd., Japan) with an

accelerating voltage of 100 kV. The TEM specimens were prepared by placing the aqueous suspension (~0.05 mg ml-1) of rGO in acetone on the copper grids followed by drying under ambient conditions. Energy-Dispersive X-ray spectroscopy (EDX) was used to do elemental analysis of the as-prepared electrodes. X-Ray Diffraction (XRD) with CuKα radiation (lambda = 1.54 Å) was employed to characterize the crystalline structure of as-prepared PdNPs. The chemical composition and the energy state of elements in rGO and as-electrodeposited Pd were carried out using X-ray photoelectron spectroscopy (XPS) measurements with Al-K alpha radiation ($h\nu = 14866$ eV).

3. Electrochemical evaluation

The electrocatalytic activity of as-prepared 3D ultraporous Pd/rGO/CFP electrode was tested in 1.0 M ethanol in 0.5 M NaOH using cyclic voltammetry (CV) at different scan rates. Chronoamperometry was used to characterize the catalytic stability of the as-prepared electrodes. All electrochemistry measurements were carried out using a computer-controlled μ-AUTOLAB II potentiostat (Eco-Chemie, Utrecht, The Netherlands) equipped with a FRA2 frequency response analyzer module running GPES/FRA software under a three-electrode system consisting of a Pt wire counter electrode, an Ag/AgCl reference electrode saturated in KCl, and a working electrode.

4. Electrodeposition of 3D ultraporous Pd nanocrystals

The PdNCs were electrodeposited onto the surface of rGO/CFP electrode using cyclic voltammetry. Cyclic voltammogrm in Fig. S1 was obtained by cycling potential from 0 to -0.75 V vs. Ag/AgCl to the rGO/CFP electrode in 1 mM $Pd(NO_3)_2$ in 0.5 M H_2SO_4 at a scan rate of 0.01 V s^{-1} for 10 cycles. During the cathodic scan, significant crystallization overpotential can be noticed before palladium electrodeposition occurs; the cathodic current density increases at potential more negative than -0.22 V vs. Ag/AgCl. The onset of the reduction peak occurs at −0.30 V vs. Ag/AgCl. At higher negative applied potential, current density increases as a linear relationship with the potential due to the hydrogen evolution. The electrodeposition mechanism of Pd during the cathodic scan is as follow, $Pd^{2+} + 2e^- \rightarrow$ Pd. On the other hand, during the anodic scan the onset of the stripping peak of Pd (Pd $\rightarrow$ $Pd^{2+} + 2e^-$) is observed at -0.15 V vs. Ag/AgCl for which it is believed that this striping process is a key leading to the ultraporous structure.

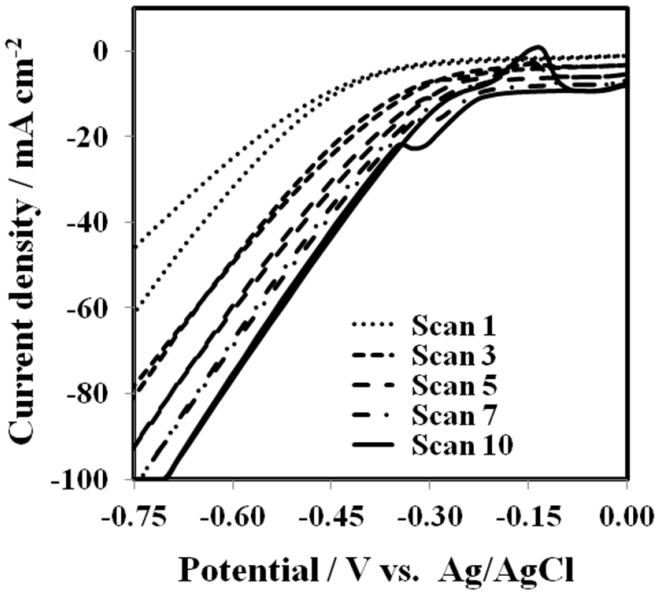

Fig. S1. Electrodeposition process of 3D ultraporous Pd nanocatalysts by cycling potential from 0 to -0.75 V vs. Ag/AgCl to rGO/CFP electrode in 1 mM $Pd(NO_3)_2$ in 0.5 M H_2SO_4 at a scan rate of 0.01 V s^{-1} for 10cycles.

5. Raman and FTIR spectra of graphene oxide (GO) and reduced graphene oxide (rGO)

The Raman spectra of GO and rGO (Fig. S2a) show the breathing mode of A_{1g}, the so-called D band, at about 1342 cm−1. The in-plane bond-stretching motion of E_{2g} of sp^2 carbon atoms, the G band, occurs at about 1576 cm−1.[1] After the reduction of GO, the intensity of the D band of rGO is higher than that of the G band due to creation of many new smaller graphitic (sp2 carbon) sheets. The intensity ratio of G/D is 0.96, which is in good agreement with previous work.[2] Fig. S2b shows the FTIR spectra of GO and rGO powders. The presence of different functionalities was found at ~3200-3400 cm-1 (a broad peak of O-H), at ~1718 cm-1 (C=O), at 1579 cm-1 (skeletal C=C), at 1226 cm-1 (C-OH), and at 1070 cm-1 (C-O). All of these observations are due to stretching vibrations. After the reduction of GO with fructose, the intensity of all peaks in Fig. S2b corresponding to the oxygen containing groups was dramatically decreased indicating that a green reducing agent fructose has capability to reduce GO. These FTIR results agree well with other previous work.[2]

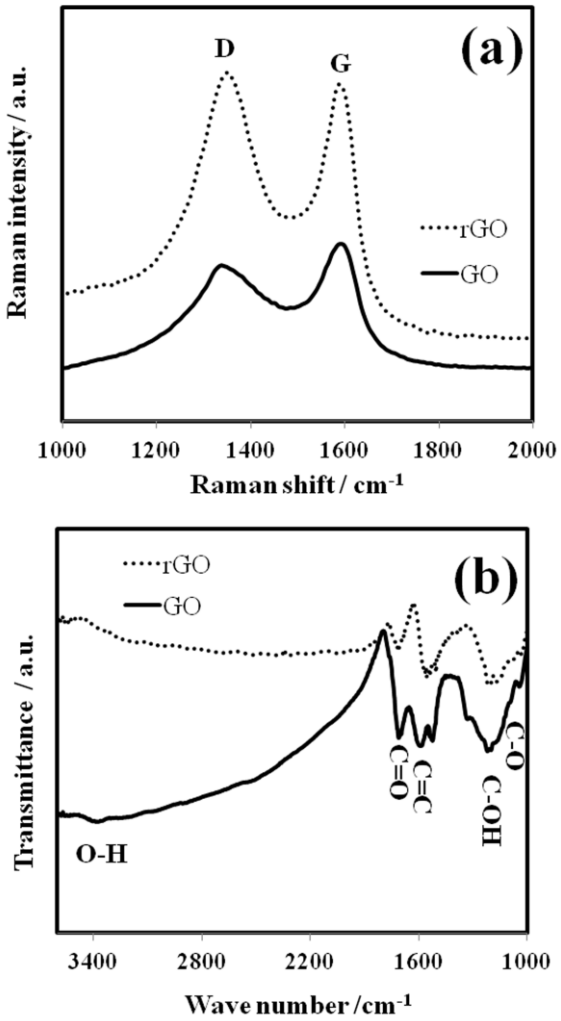

Fig. S2. (a) Raman and (b) FTIR spectra of GO and rGO nanosheets.

6. EDX and XRD spectra of Pd/rGO/CFP

The EDX spectrum of as-electrodeposited Pd on the rGO/CFP electrode shown in Fig. S3a consists of a very sharp peak at 0.28 keV associated with CK_α due to the carbon atoms of rGO and CFP, and a predominant peak at 2.84 keV from Pd$L_{\alpha 1}$ due to the Pd element.[3] A typical XRD pattern of Pd/rGO/CFP shown in Fig. S3b consists of predominant diffraction peaks at 40.00°, 46.52°, and 67.60° which are indexed to the (111), (200), and (220) planes of face-centered cubic crystalline structure. The (111) plane is found as the most common due to its having the lowest surface energy as compared to other phases. This means that the growth of electrodeposited Pd nanoclusters on rGO nanosheets favors a specific crystallographic direction of (111) plane.[4] The broad nature of the diffraction peaks is consistent with the presence of Pd nanocrystallites. In addition, the XRD patterns are in good agreement with reported data (JCPDS No. 46-1043) and previous work.[5]

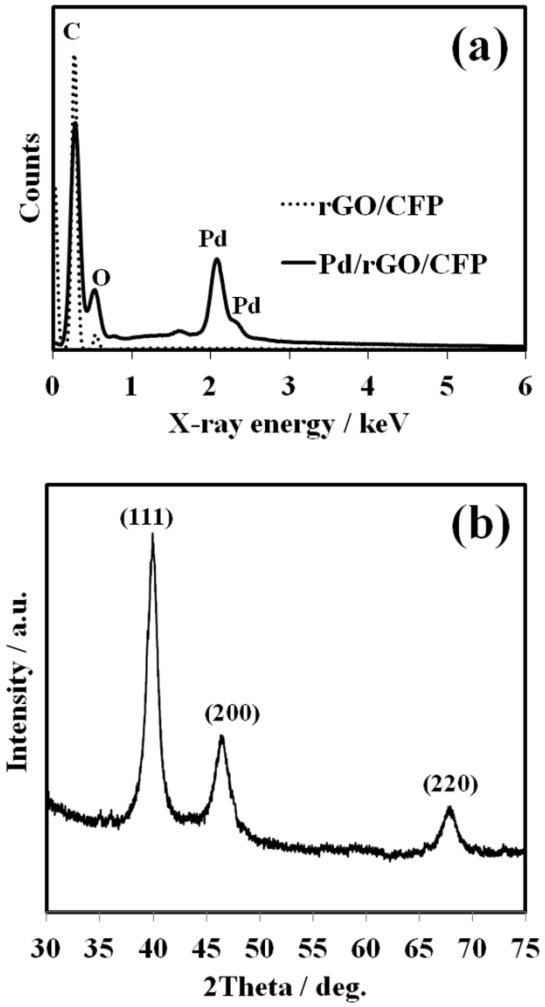

Fig. S3. (a) EDX spectra of rGO/CFP and Pd/rGO/CFP and (b) XRD pattern of Pd/rGO/CFP.

6. TGA curves of Pd/GO/CFP and Pd/CFP

TGA was used to examine the weight percentage of PdNCs and thermal decomposition of the as-prepared catalyst electrodes in air at a heating rate of 10 °C min^{-1}. The curves of weight loss and derivative weight change are shown in Fig. S4. This weight loss can be attributed to 5wt% PTFE typically used in CFP at about 540 ºC and the gaseous oxidation of carbon of rGO and CFP at about 730 ºC.[6] The residual weight corresponding to the weights of the Pd catalysts are observed to be approximately 0.36 and 0.35 mg cm^{-2} for Pd/GO/CFP and Pd/CFP, respectively. It is interesting for the case of Pd/CFP when the temperature was increased to 200 °C, a peak due to the evaporation of water was observed in Fig. S4b. This result indicates that the Pd/CFP is more hydrophilic than others, which is not good for the fabrication of DEFCs.

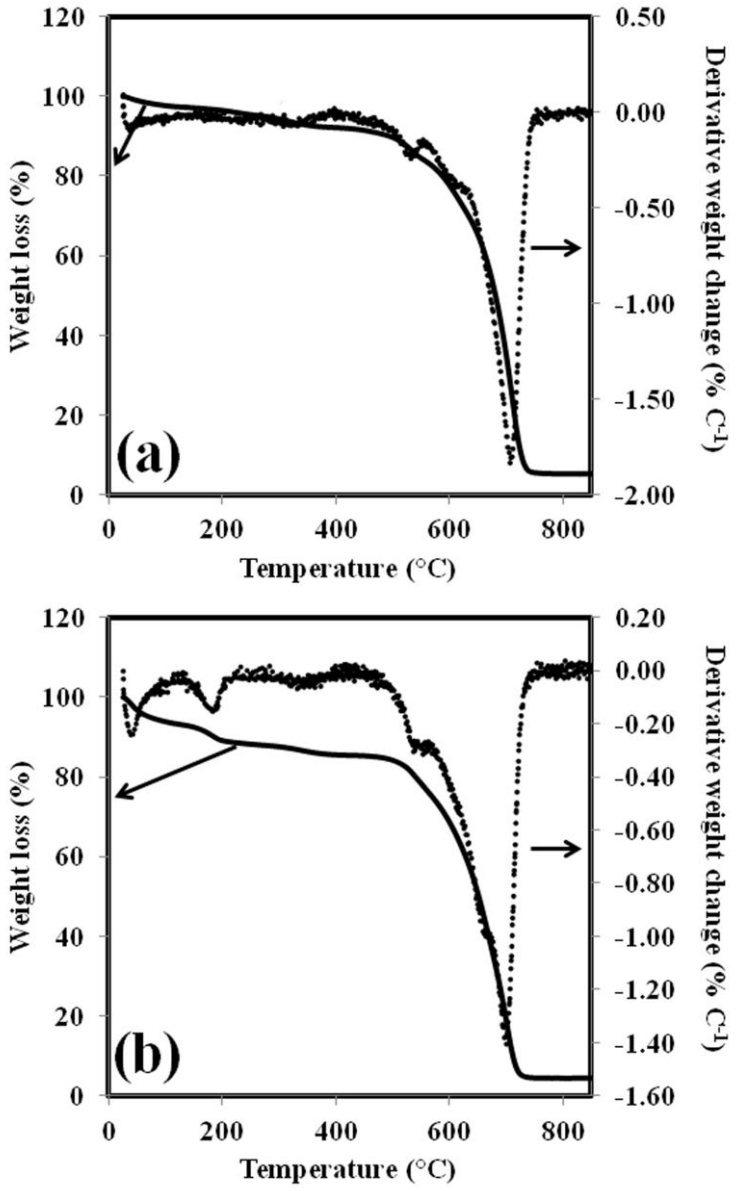

Fig. S4 TGA weight loss and derivative weight change profiles of (a) Pd/GO/CFP and (b) Pd/CFP samples.

7. Electrochemically active surface area of as-prepared electrodes

One of the most important parameters in fuel cell electrocatalysts is the real surface area of the catalyst electrode, which will determine the catalyst activity. Electrochemically active surface area (*EASA*) of as-prepared Pd-based electrodes was determined by cyclic voltammetry in 0.5 M H_2SO_4 at a scan rate of 0.01 V s^{-1} (Fig. S5) and also compared with Pd-C/CFP, Pd/GO/CFP, and Pd/CFP electrodes. The voltammetric feature of these as-prepared

electrodes in 0.5 M H_2SO_4 is from the adsorption and desorption of hydrogen within the potential range of −0.40 to 0.10 V, the double-layer capacitance region between 0.10 and 0.50 V, the formation of surface oxide at potentials more positive than 0.50 V, and the onset of the reduction of the surface oxide in the cathodic scan at 0.49 V vs Ag/AgCl. The chemisorption process of hydrogen can be used to calculate *EASA* by following equation; $EASA=Q_m/(d_m e)$ where Q_m is the charge associated with the fomation of hydrogen adsorbed/desorbed in the molayer, d_m is the surface metal atomic density, and e is the electron charge.[7] The value of d_m can be evaluated using the anderson criterion, which proposed that for the polycrytalline surfaces with low Miller index planes, d_m is about 1.3×10^{15} cm^{-2}. In this case, $d_m e$ of Pd is 0.208 mC cm^{-2}.[6, 7] The calculated *EASA* of ultraporous Pd/rGO/CFP per the weight of Pd catalyts is about 632 cm^2 mg^{-1}, which is significant higher than 258 cm^2 mg^{-1} of Pd coated on CNT.[4] In addition, the EASA of Pd/rGO/CFP is about 1.7-, 3.3-, and 5.0-fold higher than those of Pd/GO/CFP, Pd/CFP, and Pd-C/CFP (commercial catalyst), respectively.

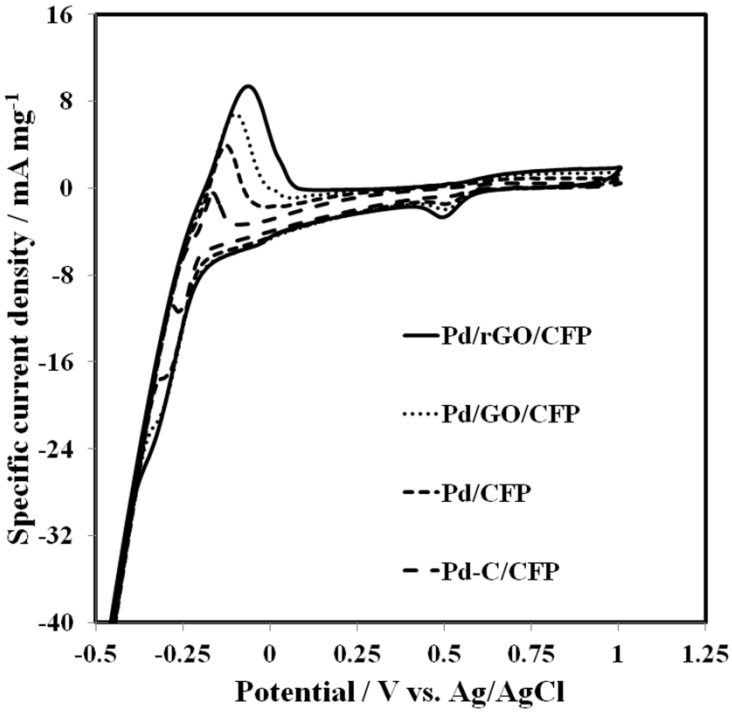

Fig. S5. All as-prepared Pd catalyst electrodes in 0.5 M H_2SO_4 at a scan rate of 0.01 V s^{-1} as compared with Pd-C/CFP.

References

1. M.-C. Hsiao, S.-H. Liao, M.-Y. Yen, P.-I. Liu, N.-W. Pu, C.-A. Wang and C.-C. M. Ma, *ACS Appl. Mater. Interfaces*, 2010, **2**, 3092.
2. X. Zhou, J. Zhang, H. Wu, H. Yang, J. Zhang and S. Guo, *J. Phys. Chem. C*, 2011, **115**, 11957.
3. G. Hu, F. Nitze, H. R. Barzegar, T. Sharifi, A. Mikołajczuk, C.-W. Tai, A. Borodzinski and T. Wågberg, *J. Power Sources*, 2012, **209**, 236.
4. C.-T. Hsieh, Y.-Y. Liu and A. K. Roy, *Electrochim. Acta*, 2012, **64**, 205.
5. Y. Zhao, X. Yang, J. Tian, F. Wang and L. Zhan, *Int. J. Hydrogen Energ.*, 2010, **35**, 3249.
6. C.-T. Hsieh, Y.-Y. Liu, Y.-S. Cheng and W.-Y. Chen, *Electrochim. Acta*, 2011, **56**, 6336.
7. J. M. Doña Rodríguez, J. A. Herrera Melián and J. Pérez Peña, *J. Chem. Educ.*, 2000, **77**, 1195.